TECHNICAL NOTE

Development of a high vacuum cantilever beam magnetometer for measurement of mechanical and magnetic properties of thin films

A. Sarkar, R. Adhikari and A. K. Das

The cantilever beam magnetometer (CBM) is an apparatus by means of which in situ measurement of the mechanical and magnetic properties of thin films can be made. We report here on the development of a cost-effective home-built CBM set-up under the high vacuum conditions and demonstrate its ability to measure intrinsic stress during the growth of magnetic/non-magnetic thin films and thereafter the magnetization of the magnetic films as a function of the magnetic field. The reproducible performance of the set-up has been demonstrated with various magnetic and non-magnetic films deposited on the p-Si(100) substrates.

Over the past few decades, the evolution of thin film technology and its ubiquitous influence on all aspects of science has been a landmark for researchers. From computer systems, to the refinement of optical devices (viz. mirrors, filters, etc.), solar cells, protection against corrosion and tribology, thin films have grasped the very root of modern-day technology. With the advancement of very large-scale integration (VLSI) technology, thin films are present in all aspects of modern-day electronic devices. The fabrication of electronic devices involves deposition of thin films by various techniques, e.g., physical or chemical vapour deposition, sputtering (DC and RF), electrochemical and spin-coating deposition, thermal and electron beam evaporation (EBE), etc. Regardless of the technique of preparation, thin films develop a large intrinsic stress during the course of their deposition, which sometimes has values that even exceed the tensile strength of the respective bulk phases[1]. This embarks one of the greatest and unavoidable challenges in thin film technology. The malfunctioning or even failure of thin films in technical applications is often due to mechanical stresses built during or after their preparation. In the worst case, the mechanical stresses can even cause the films to rip open or peel their substrates[2,3]. Thus, in order to improve the reliability of thin film-based devices, a better understanding of the mechanical stresses and the preparation techniques is required to optimize the stresses in thin films. Apart from the technological point of view, such studies are also interesting scientifically. Measurement of the film stresses provides information on how the growth parameters influence the stresses in thin films. The growth morphology and intrinsic stress of thin films seem to have a strong correlation[4,5]. A number of stress measurement techniques[6–8] have been used for measuring the intrinsic stress of materials. However, the cantilever beam technique has been commonly used for stress measurements during as well as after the film deposition[9–14] and has also been successfully employed to study the relation between the intrinsic stress and the microstructure and growth mode of numerous polycrystalline[15] and epitaxial[16] thin films.

From the technological perspective, magnetic thin films have attracted tremendous attention for decades and have been studied extensively due to their unmatched applicability for the storage technology[17]. Several measurement techniques with enhanced surface sensitivity have been employed for the study of magnetic properties such as magnetization, Curie temperature or magnetic anisotropy of thin films. The torsion oscillation magnetometer (TOM)[18], Mössbauer spectroscopy[19], ferromagnetic resonance[20], surface magneto-optic Kerr effect (SMOKE)[21] and the superconducting quantum interference device (SQUID)[22] have been commonly used to measure the magnetic properties of thin films, even of a few monolayers. Most of the magnetometers are designated for measuring some particular aspect of magnetic materials. The cantilever beam magnetometer (CBM)[23,24] is versatile in the sense that it can measure most of the aspects of the magnetic thin films, including the mechanical stresses with submonolayer sensitivity. In addition, CBM is suitable for *in situ* measurements. Stress measurements (intrinsic and/or magnetostrictive) make CBM unique compared to other magnetometers.

The CBM is based on the simple cantilever beam theory. A conducting (or semiconducting) substrate in the form of a cantilever plate is fixed at one end and the deflection of the free end, which is proportional to the film stress or the magnetization, is determined with a high sensitivity and long time stability using a differential capacitance method[23] in combination with a phase-sensitive detection or optical method[24]. During the course of deposition of a thin film over a cantilever substrate, a large stress may develop due to numerous mechanisms, viz. lattice mismatch, thermal expansion difference, grain-boundary relaxation, recrystallization processes, capillary effect, etc. Depending on the type of mechanism, the stress induced in the substrate is either tensile or compressive. However, the intrinsic stress (σ_{int}), thus developed, would administer a force over the cantilever substrate and as a result, the free end of the substrate may deflect or bend. Similarly, if the deposited film is magnetic in nature, torques ($\vec{T}_{\text{m}} = \vec{m} \times \vec{B}_{\text{defl}}$) act on the magnetic moments ($\vec{m}$) of the film under the influence of an external magnetic (deflecting) field ($\vec{B}_{\text{defl}}$), which may again lead to the bending of the cantilever substrate. Thus, the quantitative values of the involved forces (stress) or torques (magnetization) can be determined by measuring the amount of deflection of the free end of the cantilever substrate. So, the main task in the CBM experiment would be the measurement of deflection of the cantilever substrate with higher resolution and sensitivity. Koch and his coworkers[16,23] have demonstrated a lock-in assisted differential capacitance technique as an efficient way to measure the deflection of the cantilever substrate, where the free end of the cantilever substrate is kept between two parallel plates of a capacitor, as shown in Figure 1. An AC voltage of 28.8 kHz frequency is supplied to the capacitor plates, and a reference signal of the same frequency is

supplied to the lock-in-amplifier. The cantilever substrate is kept in floating ground, which acts as a common (capacitor) plate. When the substrate is equidistant from the top and the bottom plates, the system is considered to be in the initial condition where the net induced charge on the substrate is null. Now for any deflection (Δ) of the cantilever substrate from its equidistant position between the plates, there would be a net induced charge on the substrate, which results in the flow of current through it. This current is then converted into voltage using an *I–V* converter-cum-preamplifier and finally, the amplified voltages (V_{LI}) are detected by the lock-in-amplifier. Since it is practically impossible to place the substrate exactly at equidistant position from the capacitor plates, a CBM control unit is used to initialize the current/voltage signal coming from the substrate to zero at the starting point by controlling the relative voltage supplied to the top and the bottom capacitor plates. The CBM control unit primarily consists of a voltage divider circuit with RC oscillator to control the phase of the voltage (AC) given to the capacitor plates. The deflection (Δ) is derived from the measured lock-in-voltage (V_{LI}) through the relation

$$\Delta = \frac{\Delta_{cal}}{V_{LI,cal}} V_{LI}, \quad (1)$$

where $V_{LI,cal}$ is the lock-in-voltage due to a known deflection of Δ_{cal}, which could be the deflection of the free end of the cantilever substrate due to its own weight.

The CBM is not commercially available unlike other magnetometers. Few laboratories in the world have developed such CBMs for their own research purposes[23–27]. In our laboratory, we have developed a CBM set-up under high vacuum (HV) environment. The set-up consists of the following components: (i) custom-designed HV chamber and electron beam evaporator; (ii) designed and fabricated cantilever substrate holder (CBM device) with proper electrical arrangements and (iii) a pair of Helmholtz coils (HCs) fabricated and placed between the poles of an electromagnet (EM) for perpendicular magnetic field. We then assembled all components and automated data acquisition using LABVIEW programing. We made the set-up operational and demonstrated the measurements of intrinsic stress and magnetization of some standard metallic thin films deposited on Si(100) substrates.

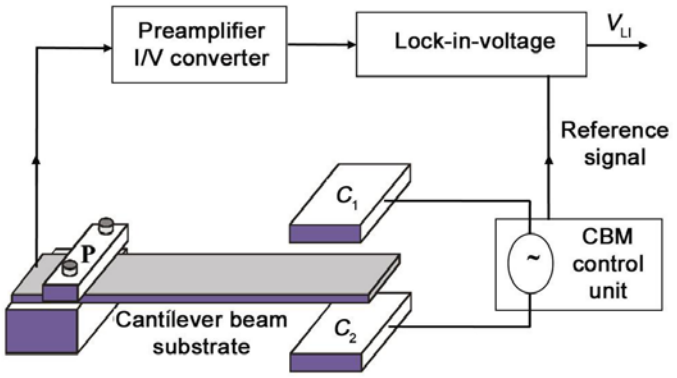

Figure 1. Schematic diagram of a cantilever beam magnetometer (CBM) device with electrical connections for the measurement of cantilever deflection. C_1 and C_2 represent the upper and lower capacitor plates and *P* is the substrate holder from where the signal is being derived. V_{LI} is the output lock-in-voltage.

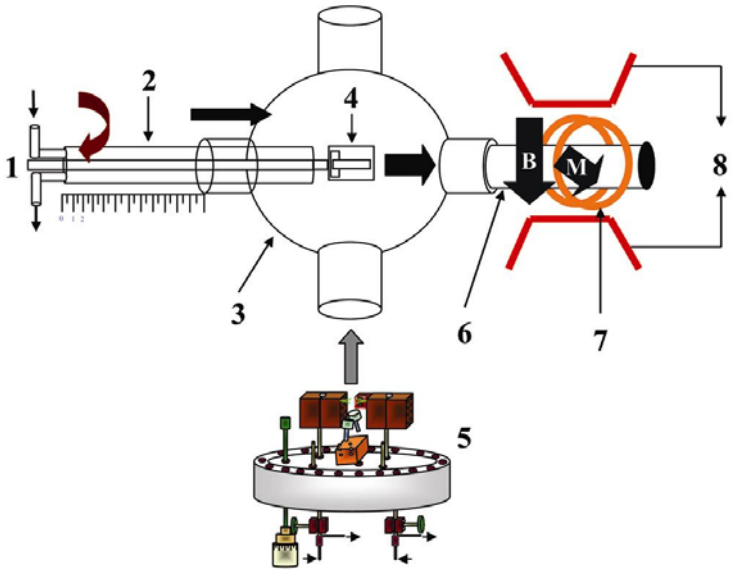

Figure 2. Schematic representation of the CBM set-up with (1) water and electrical feed-through; (2) manipulator rod; (3) high vacuum (HV) chamber; (4) CBM device; (5) evaporator; (6) non-magnetic hollow tube; (7) electromagnet pole pieces, and (8) pair of Helmholtz coils.

Instrumentation

A schematic representation of the full CBM set-up is shown in Figure 2. It gives a clear view of the different components and how they are bridged. The design of the HV chamber is crucial for the abridgement of the CBM device on the manipulator, the evaporator and the electromagnetic system which produces orthogonal magnetic fields. A substrate (in a cantilever form) on which the film will be deposited, is loaded in the CBM device; the device is then inserted at one end of the manipulator which has rotational and translational degrees of freedom. The manipulator is mounted on the HV chamber through a flange. The electrical connections of the CBM device are taken out from the HV to air through electrical feed-through from the other end of the manipulator. Using manipulator, the CBM device carrying the substrate is placed on top of the evaporator (which is attached to the bottom flange of the HV chamber) for deposition of thin films. During deposition, the deflection/bending of the substrate is measured

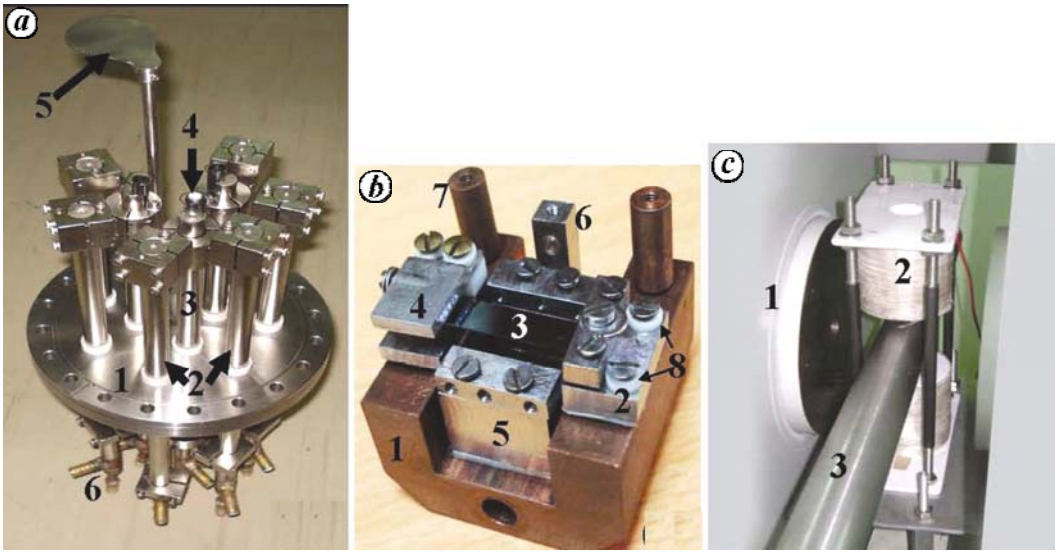

Figure 3. Image of the fabricated ***a***, e-beam evaporator with (1) conflate flange; (2) copper electrodes for the filament; (3) copper anode; (4) material for deposition; (5) shutter and (6) water feedthrough to cool the evaporator. ***b***, Cantilever beam device with (1) U-shaped copper base; (2) substrate holder arrangements; (3) cantilever substrate; (4) capacitor plates; (5) substrate heater arrangements; (6) thermocouple holder; (7) mask holder and (8) insulating ceramic ring/plates. ***c***, Arrangement of the electromagnet (1) and the Helmholtz coil (2) to produce orthogonal magnetic fields at the sample site placed inside the non-magnetic tube (3).

to monitor the stress evaluation in thin films. For magnetic characterization of the film/substrate composite, the CBM device is placed at the centre of the orthogonal magnetic field by translating the device through a non-magnetic tube (which is attached to the flange located exactly opposite another flange for the manipulator in HV chamber) with the help of the manipulator without breaking the vacuum condition. Thus all measurements in this set-up are performed *in situ*, i.e. the growth and characterization are under the same environment. Proper instrumentation is needed to fulfil the requirements. All the components of the CBM unit have been machined from non-magnetic stainless steel (SS), unless mentioned otherwise. We briefly discuss the design and fabrication of different components of the set-up.

HV chamber

It is a spherical chamber with inner diameter (i.d.) of 300 mm and has all the necessary provisions required for ultra high vacuum (UHV) conditions. Oil-free turbo molecular pump and rotary vane pump are used to achieve a vacuum level of 10^{-7} mbar of the chamber and a dual range compact vacuum gauge is attached for monitoring the vacuum level. The chamber is mounted over a metal stand along with the manipulator and is aligned properly so that the manipulator (along with the CBM device) can pass freely through the centre of the chamber.

Evaporator

For deposition of thin films, the HV chamber is also equipped with three EBE sources and a quartz crystal oscillator for thickness estimation. The three compact EBE sources (Figure 3 *a*) are fabricated on a 150 mm i.d. conflate flange which is attached at the bottom of the HV chamber as indicated in Figure 2. In order to reduce the thermal effect on other parts of the chamber, the EBE sources are shielded by water-cooled SS plates along with additional tantalum and copper shielding. This is not exactly a conventional electron beam evaporator. We have designed it in such a way that a high positive voltage (~ 1 kV) is being applied to the crucible (through the anode) where an isolated filament surrounds it. A high current (0–30 A) is passed through the filament resulting in the emission of electrons which are accelerated and collected by the crucible (anode). The electrons on bombardment with the crucible heat it up and as a result the material kept inside the crucible is evaporated. Due to the difference in pressure around the cantilever substrate (at the centre of the chamber) and the crucible, the evaporated material tends to move towards the lower pressure region and as a result deposition over the substrate takes place. In our system we have three such crucible arrangements so that we can, simultaneously or one after another, evaporate three types of materials and have a layer/multilayer film of the desired thickness. We have used tungsten and molybdenum for making the crucibles due to their high melting point. Thoriated tungsten wire of 0.25 mm diameter is used for the filament due to its low work function and high melting point. The electrodes are made of copper rods for their good thermal and electrical conductivity, which have water cooling provision to cool the electrodes during deposition.

Manipulator

This is a double-walled hollow cylindrical rod of length 150 cm and has the necessary electrical and liquid feed-through. It can be rotated (through 360°) and linearly translated (through 70 cm) manually within the HV chamber with a best vacuum of 5×10^{-6} mbar. The degrees of freedom of a manipulator are important for placing the CBM device in proper experimental geometry required for the measurement of magnetization, magnetocrystalline anisotropy and magnetostriction. However, limited degrees of freedom of our manipulator restrict the

measurement of magnetocrystalline anisotropy and magnetostriction.

CBM device

It is the heart of the magnetometer. Figure 3 *b* shows a photograph of the fabricated CBM device. It consists of a U-shaped copper base ($35 \times 35 \times 20$ mm) with greater heights (10 mm) on both sides (labelled as (1) in the figure), all the arrangements for holding the clamps (2) of the cantilever substrate (3), metal plates (4) of the capacitor, heating foil (5), thermocouple holder (6), mask holder (7) and detachable electrical connections. A hole of diameter 4 mm in the copper base (see bottom of the figure) is used to attach the device on the manipulator using nut and bolt arrangement. As the copper base is directly connected to the water-cooled manipulator, it becomes important to isolate all the arrangements (mentioned above) electrically from the copper base. This is done using ceramic plates and rings machined at proper dimensions. On the manipulator, there are host electrical connectors which connect the CBM device at one end (inside the HV chamber) and the instruments (power supply, CBM control unit, lock-in-amplifier, etc.) on the rack through the electrical feed-through at the other end. The copper base was chosen for better thermal conductivity to exploit the water-cooled manipulator as a heat sink for the CBM device. The cantilever substrate (Si-wafer of dimension $25 \times 5 \times 0.15$ mm) is clamped on one side of the base by two metal plates to guarantee uniform distribution of the clamping force onto the substrate. This arrangement helps to avoid breaking of the thin cantilever substrate either during clamping or for experiments at elevated temperatures. The clamping end of the substrate is electrically isolated from the copper base by putting the ceramic plate and rings in appropriate places. The free end of the cantilever substrate acts as a common capacitor plate between two stationary metal capacitor plates ($15 \times 9 \times 3$ mm) which are fixed on the other side of the copper base. A ceramic spacer of 3 mm height is used to isolate the stationary capacitor plates from each other and as a whole they are electrically isolated from the base. The plates are fed with AC voltage from a CBM control unit. The signal, generated due to bending of the cantilever beam, is collected from the substrate and is fed into the lock-in-amplifier via the pre-amplifier. For measurement at a higher temperature, the heating is achieved by radiation from a heater (2 μm thick tantalum heating foil) which is placed just below the cantilever substrate and electrically isolated from the base. A K-type (chromel–alumel) thermocouple is placed just at the site of the substrate with the help of a holder (marked (6) in Figure 3 *b*). For each experiment, we have to load a new cantilever substrate in the CBM device and then carefully mount it on the manipulator and make one-to-one electrical contacts between connectors on the CBM device and on the manipulator.

Electromagnetic system

For magnetic measurements, soon after the deposition of thin films, the CBM device is translated through the non-magnetic tube and placed at the centre of two orthogonal magnetic fields. A high field (–2T – 0 – +2T) from Bruker EM is used to magnetize the sample (henceforth called the magnetizing field H_m). The required deflecting field ($\vec{B}_{defl}$) is provided from a pair of indigenously built HCs, powered by a programmable KEPCO BOP supply. The HCs are placed inside EM such that they provide an orthogonal magnetic field at the site of the cantilever substrate shown in Figure 3 *c*. Care has to be taken so that either field should not be affected by the other.

Electrical connections and programing

Any deflection of the cantilever beam is marked by the change in the capacitance which is measured in terms of the change in voltage with the help of a pre-amplifier-cum-current (I)–voltage (V) converter (DLPCA-200, FEMTO). Signals are transferred using shielded BNC cables. Data acquisition is performed by acquiring and storing data from a DSP lock-in-amplifier (signal recovery). While measuring stress, the system stores data continuously at an interval of 5 sec till completion of deposition. A personal computer (Pentium-IV) having NI GPIB IEEE 488.2 card has been used to acquire data through LABVIEW programing.

A complete photograph of the fabricated CBM is shown in Figure 4 with all necessary parts assembled together.

Calibration

After assembly, we have calibrated the CBM set-up in few steps. From eq. (1), we can see that in order to measure deflection (Δ) we must first calibrate the voltage readings of the lock-in-amplifier (LI). Initially the CBM device along with the cantilever substrate between two parallel plate capacitors is kept vertical to the plane of the floor (i.e. the surface normal to the substrate is parallel to the floor). Under such conditions the AC voltage applied to the capacitor plates is adjusted to get zero LI voltage reading. Now the CBM device is rotated through 90° such that the cantilever substrate becomes horizontal to the plane of the floor (i.e. the surface normal to the substrate is perpendicular to the floor). This would cause the cantilever substrate to deflect (Δ_{cal}) between the capacitor plates due to its own weight and produce a corresponding change in the LI voltage ($V_{LI,cal}$). Thus rotating the CBM device in steps through 360° would produce voltage change as shown in Figure 5 with the peak voltage of $V_{LI,cal}$ corresponding to the deflection of the substrate due to its own weight, which is given by

$$\Delta_{cal} = \frac{3}{2}\frac{\rho_s g l_s^4}{Y_s t_s^2}, \tag{2}$$

where ρ_s, Y_s, l_s, t_s are mass density, Young's modulus, length and thickness of the substrate respectively, and g is the acceleration due to gravity. Any further change in the deflection (Δ) due to stress or magnetization can be easily obtained from eq. (1) by measuring the subsequent lock-in-voltage (V_{LI}). To maximize the sensitivity of measurements, one needs to repeat this calibration to find $V_{LI,cal}$ at the beginning of any experiment.

We have calibrated current (I) versus magnetic field (H) for the EM and HCs. The I–H calibration for EM and HCs is shown in Figure 6 *a* and *b* respectively. It is to be mentioned here that the data presented in Figure 6 are recorded for the flat pole configuration of EM with a pole separation of 55 mm. For HCs, the separation was about 85 mm. The production of uniform magnetic field by HCs over the required dimension defined by the cantilever substrate was verified. It is important for all magnetic measurements in the CBM set-up that the deflecting magnetic field produced by the HCs

Figure 4. Image of the assembled CBM consisting of the manipulator with necessary electrical and water feed-through (1), high vacuum pumps (2), HV chamber (3), evaporator (4), non-magnetic hollow tube (5), electromagnetic system (6), CBM control unit (7) and personal computer for acquisition and processing data (8).

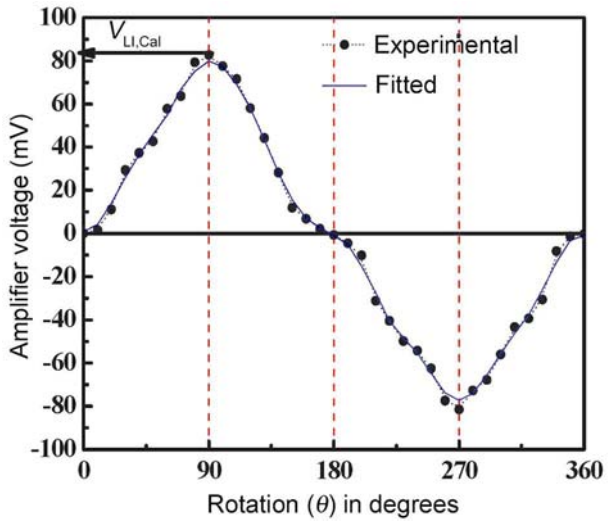

Figure 5. Calibration curve obtained by rotating the manipulator in steps through 360° to determine $V_{LI,Cal}$.

(B_{defl}) should be stable and unaffected by variation in the magnetizing field (H_m) produced by the EM. A study of this stability is presented in Figure 6 *c*. To measure the temperature we have used a thermocouple which was calibrated (Figure 6 *d*). Finally, the thickness of the deposited film with deposition time and rate was calibrated by verifying the measured thickness for many samples using variable angle Stokes ellipsometer (model: L116S, Gaertner Scientific Corp., Chicago).

After calibrating the cantilever beam apparatus, we have demonstrated the capability of the instrument in measuring the intrinsic stress and the magnetization of thin films of some standard materials such as iron (Fe), cobalt (Co) and silver (Ag). The films (l_f = 19 mm, $w_f = w_s$ = 5 mm) were deposited on the p-Si (Y_s = 185 GPa, ν_s = 0.28, t_s = 130 μm and l_s = 25 mm) substrates at two different substrate temperatures (T_s = 30°C (room temperature) and 100°C). The corresponding values of the intrinsic stress (σ_{int}) and magnetization (M) have been determined from the measured deflection (Δ) using simple relations, which we derive briefly in the following section.

Relation of deflection with intrinsic stress and magnetization

As mentioned earlier, the main task in CBM experiments is to measure the deflection of the cantilever beam substrate on which films are deposited. Then one can determine the intrinsic stress (σ_{int}) and magnetization (M) from the measured deflection (Δ), if relations among them are known. Let us consider a bimorph (film/substrate) system as shown in Figure 7 *a*, which consists of a very thin film (thickness = t_f, width = w_f and length = l_f) deposited on a substrate (thickness = t_s, width = w_s and length = l_s). For simplicity in calculation, we assume that $t_f \ll t_s \ll w_s$ (= w_f) < l_s (≠ l_f). According to the cantilever beam theory[28], there is a certain neutral plane above and below which the surfaces of the cantilever get elongated (contracted) and contracted (elongated) respectively. It is well known that the bending of a cantilever beam due to external torque (T_{Ext}) or force with respect to (w.r.t.) the neutral plane is balanced by an internal bending moment (T_B) due to restoring force w.r.t. the same neutral plane, such that

$$T_B + T_{Ext} = 0 \quad \text{or} \quad T_B = -T_{Ext}. \qquad (3)$$

The origin of the external torque may be either the intrinsic stress (σ_{int}) of the film or the magnetization (M) of the film in an external magnetic field ($\vec{B}_{defl}$). As origin of both the torques is totally different, we need to treat the cases separately.

The internal bending moment (T_B) of a cantilever beam can be written as EI/R, where E is the elastic modulus, I the geometrical moment of inertia and R is the radius of curvature of the cantilever. Now, for small bending, $1/R$ can be taken as d^2z/dx^2, where length (width) of the cantilever is along the x-axis (y-axis) and deflection is along the z-axis. Then the internal bending moment (T_B) is given by $EI(d^2z/dx^2)$ and can be equated to the external torque ($T_{Ext} = T_m$ or T_σ from eq. (3))

$$EI\frac{d^2z}{dx^2} = -T_{Ext}. \qquad (4)$$

Solving eq. (4) under appropriate boundary conditions (experimental geometry), one can get slope [$\tan\theta = (dz/dx)$] and deflection [$\Delta = z(x)$] at any measurement point, say x on the cantilever substrate.

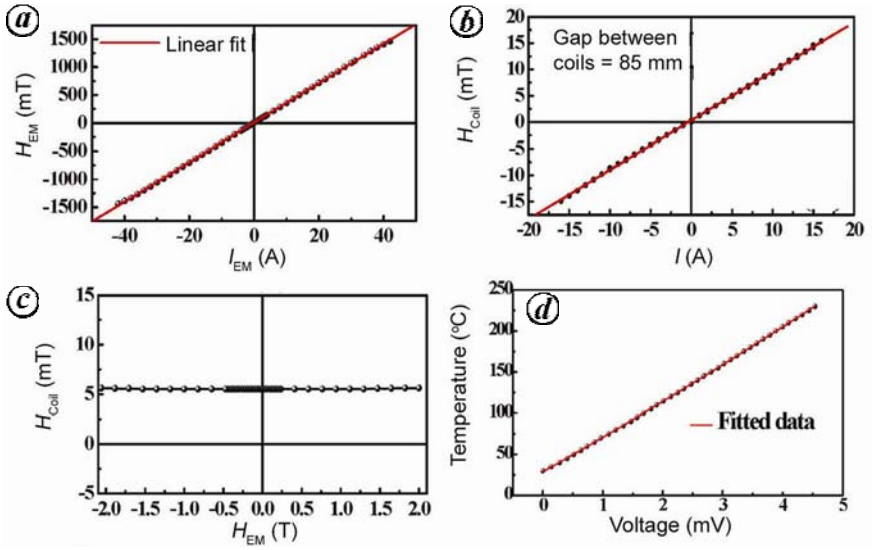

Figure 6. Calibration curve for (***a***) electromagnet field, (***b***) field produced by the Helmholtz coils, (***c***) effect of the electromagnet field on the Helmholtz coil field and (***d***) thermocouple.

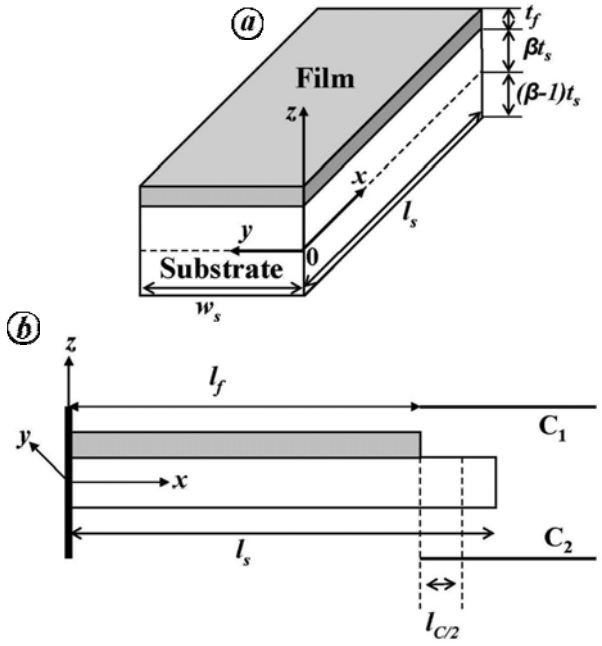

Figure 7. Film/substrate bimorph system with parameter notations and geometric directions of the cantilever substrate with thin film, where (***a***) shows the position of neutral plane and (***b***) shows the position of the cantilever substrate in capacitor plates.

A schematic diagram of cantilever bending with parameter notations and directions is shown in Figure 7 *b*.

Intrinsic stress

In this case, the bending of the beam is caused by the torque experienced due to the force that acts at the film–substrate interface. This force causes the bimorph to be deformed into a shell producing an isotropic biaxial stress ($\sigma_l = \sigma_w$) along the length (σ_l) and width (σ_w). The elastic modulus under such a condition is given by

$$E = \frac{Y_s}{1-\nu_s}, \tag{5}$$

where Y_s and ν_s are the Young's modulus and Poisson's ratio of the cantilever substrate respectively. Trémolet *et al.*[29] showed from energy minimization calculation that for a strained bimorph system (as in the present case), the neutral plane is shifted from the mid level to within the substrate at a distance βt_s from the film–substrate interface (strained surface). The factor β is 2/3 for a strained surface, whereas for an unstrained surface (flat interface) $\beta = 1/2$, i.e. at the mid level of the beam. Thus, for a polycrystalline film deposited on an isotropic substrate, the torque due to the forces acting at the film–substrate interface is given by: $T_{Ext} = T_\sigma$ = force in sample × distance of film surface from neutral plane in substrate, i.e.

$$T_\sigma = (\sigma_f w_f t_f) \times (\beta t_s + t_f). \tag{6}$$

For such a system the geometrical moment of inertia w.r.t. the neutral plane can be found from the following integration

$$I = \int_{(\beta-1)t_s}^{\beta t_s + t_f} wz^2 \, dz$$

$$= \frac{w}{3}[(\beta t_s + t_f)^3 - (\beta t_s - t_s)^3], \tag{7}$$

where w is the common width of the sample (w_f) and the substrate (w_s) interface. Now one should adopt I with the experimental geometry. Considering $t_f \ll t_s$ and $\beta = 2/3$, and replacing I, E and T_{Ext} ($= T_\sigma$), in eq. (4), we get the intrinsic stress in terms of the deflection as

$$\sigma_{int} = \sigma_f = -\frac{Y_s t_s^2}{3(1-\nu_s)t_f} \times \frac{\Delta}{(2l_{C/2} + l_f)l_f}, \tag{8}$$

where $l_{C/2}$ is half of the length of the cantilever substrate inside the capacitor plates (where the average measurement point is considered).

Magnetization

In this case the bending of the cantilever substrate occurs due to the torque experienced by the magnetic film in the presence of an external magnetic field ($\vec{B}_{defl}$), applied perpendicular to the plane of the film. The origin of the torque here is due to the coupling force ($= |m| \times \vec{B}_{defl}$) acting at the two ends of

the film. The film–substrate interface does not play any role in determining the bending torque, except the fact that the film is attached to the substrate and rotates along with the film. Thus the elastic modulus will be the same as the Young's modulus of the substrate (Y_s) and the neutral plane of the film/substrate system will be at the mid level of the substrate ($\beta = 1/2$). Considering this, the geometrical moment of inertia (I) would be equal to $wt_s^3/12$. Now a magnetic torque is produced for a film (volume = V_f) magnetized along the x-axis (M_x) in a perpendicular magnetic field along the z-axis (B_z)

$$T_{\text{Ext}} = T_{y,\text{m}} = -V_{\text{f}} M_{\text{x}} B_{\text{z}} \qquad (9)$$

Replacing eq. (9) in eq. (4) and proceeding like previous case, we get the magnetization of the film in terms of measured deflection as

$$M = M_{\text{x}} = \frac{Y_{\text{s}} w t_{\text{s}}^3}{2V_{\text{f}} B_{\text{z}}} \frac{\Delta}{l_{\text{f}}(2l_{\text{f}} + 3l_{\text{c/2}})}. \qquad (10)$$

Equations (8) and (10) are used for the calculation of σ_{int} and M measuring V_{LI} and determining Δ from eq. (1).

Results and discussion

Intrinsic stress measurement

Figure 8 *a–c* shows the variation of intrinsic stress in terms of film force per width (F/w) during and after deposition of Fe, Co and Ag films respectively, as a function of thickness and deposition time. It is to be noted that the film force depends linearly on the thickness (t) for constant stress ($F/w = \sigma t$). Thus the value of the intrinsic stress developed in the film could be easily evaluated from the slope of the stress-thickness versus thickness curve. The axis on the right-hand side of all the plots shows the measured deflection (calculated from eq. (1)) for each step of the measurements. The plot is divided into three distinct regions using two dotted lines. At the start of each experiment, keeping the shutter of the evaporator closed (i.e., no deposition is taking place), the system is stabilized initially for a few seconds (region 1). Then the shutter is opened (i.e., deposition is taking place) and the measured data are represented by region 2. At the end of the experiment the shutter is again

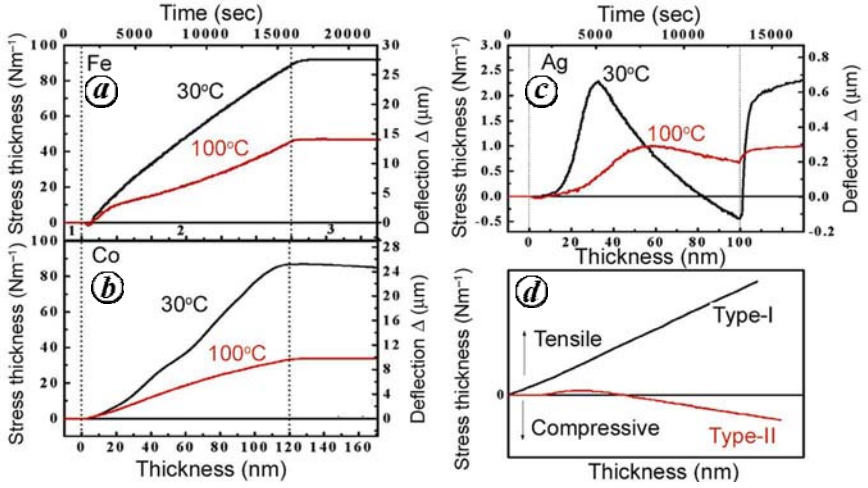

Figure 8. Experimental data of intrinsic stress in terms of stress–thickness product versus thickness (deposition time) for (***a***) Fe, (***b***) Co and (***c***) Ag measured at T_s = 30°C (room temperature) and 100°C; the dotted lines separate three regions according to the OFF (region 1 and 3) and ON (region 2) state of the shutter. (***d***) Schematic representation of the stress versus thickness curves of high melting point (type I) and low melting point (type II) materials.

closed (i.e. no deposition is taking place) and data collection is continued in this state for few more seconds (region 3). All the measurements were done for films deposited at two different substrate temperatures (T_s = 30°C and 100°C).

For Fe film deposited at room temperature, during initial stage of deposition a compressive stress (~–0.5 GPa) is observed in the thickness range 5 ± 2 nm. As the thickness of the film is increased, there is a change in the nature of the stress and tensile stress is developed in the film which reaches a value of 0.85 GPa at a thickness of 30 ± 5 nm. This tensile stress is then saturated with an average value of 0.80 GPa till the end of deposition, after which the stress remains almost constant with a slight decrease due to strain relaxation within the film. Fe and Co show a similar stress curve with tensile stress dominating for almost the whole thickness range. Similar nature of the stress-thickness curve is obtained for both Fe and Co films deposited at T_s = 100°C, but with lower magnitude of the stress values.

However, the Ag film shows a stress curve of different nature. For films deposited at room temperature, the compressive stress at the initial stage of deposition is observed with a magnitude of –0.01 GPa, but the tensile stress reaches a maximum value of 0.073 GPa at a thickness of 30 ± 5 nm. After this, there is a relaxation of the stress due to further deposition of the film until the net compressive stress again reappears with magnitude of –0.0044 GPa at a thickness of 100 ± 5 nm. At the end of deposition there is an onset of large tensile stress which saturates within a short interval of time. Whereas for films deposited at T_s = 100°C maximum tensile stress (0.02 GPa) is observed at a thickness of 47 ± 5 nm, which relaxes on further deposition but does not become compressive. The nature of stress behaviour after deposition is similar as that observed for the substrate at room temperature.

All the observed stress behaviour as a function of thickness can be classified into two groups as demonstrated schematically in Figure 8 *d*. Basically mobility of the evaporated atoms on the substrate plays an important role in deciding the nature of the stress behaviour, which can be correlated with two different modes of island growth (Volmer–Weber). The typical curve of type-I is observed for the high melting point materials having low adatom mobility (Fe, Co, Cr, etc.) and exhibits monotonous tensile stress with increasing film thickness, which is basically the characteristic of columnar grain growth. While for low melting point materials having high adatom mobility (Ag, Al, etc.), the total film stress is normally considerably smaller, and tensile as well as compressive stresses are sequentially built up with increasing film thickness. The resulting stress curve is of type-II, which is characteristic of island growth accompanied by additional lateral grain growth in continuous films. The morphology of the film can be derived con-

sidering the model[30] based on the behaviour of the intrinsic stresses as a function of thickness and temperature.

The evolution of stress in thin films during growth starting from the nucleation of islands, their coalescence upon growth and further growth of continuum film with grain structure is a complex phenomenon where stress behaviour depends on the material system and growth parameters. However, some general qualitative understanding can be achieved. A common growth mode of polycrystalline thin films is the Volmer–Weber mode. It is well known that this growth mode comprises three different growth stages: (a) the precoalescence stage where isolated islands nucleate and grow, (b) the coalescence stage where islands merge and percolate and the remaining channels are filled and (c) followed by the growth of continuum film thereon. At the initial stage of film growth, atoms nucleate over the surface and form isolated islands. The lattice parameter of isolated metal particles is expected to be smaller than that of the respective bulk phase due to capillarity effect (surface tension). As the particle nucleates and grows, the equilibrium lattice parameter increases and gradually tries to approach the respective bulk value; but this is inhibited as the particles are anchored to the substrate by adhesion. This develops a compressive strain within the particle due to the constraints (since it is adhered on the substrate surface) in expansion of the crystal lattice upon particle growth, identified by the initial dip at the start of deposition. Due to subsequent growth, the isolated islands grow and majority of the lattice expansion strain is continuously relaxed because of the weak film/substrate adhesion which is not strong enough to withstand the compressive stress. As the surface free energies of the isolated islands could be reduced by formation of common surface (grain boundary), if created by coalescence[2,10,31], the islands are snapped together (zipping effect) and generate a tensile stress within the continuous network of the islands because of forming the grain boundaries. In polycrystalline films these grain boundaries acts as an atomic sink and have reduced atomic density. The behaviour of stress during growth of the films after coalescence of islands depends greatly on the mobility of the deposited atoms. For materials having low adatom mobility (type-I), the rate of diffusion on the surface of the growing film is low compared to their rate of arrival from the vapour. As a consequence, further growth takes place over a strained system resulting in continuous growth of the tensile stress. When the deposition is stopped the tensile stress tends to saturate. If the mobility of the atoms on the growing surface is large compared to their rate of arrival (type-II), the atoms could diffuse into the grain boundaries and relax the tensile stress. Thus tensile stress is developed until a certain thickness, after which it decreases with increasing thickness of the film. At the end of deposition large tensile stress is developed due to the recrystallization process which increases the average grain size of the film. This stress then saturates within a short interval of time. The elevation of the substrate temperature basically enhances the mobility of the atoms over the surface of the substrate, thus relaxing the stress. A pictorial representation of the above phenomenon is given in Figure 9.

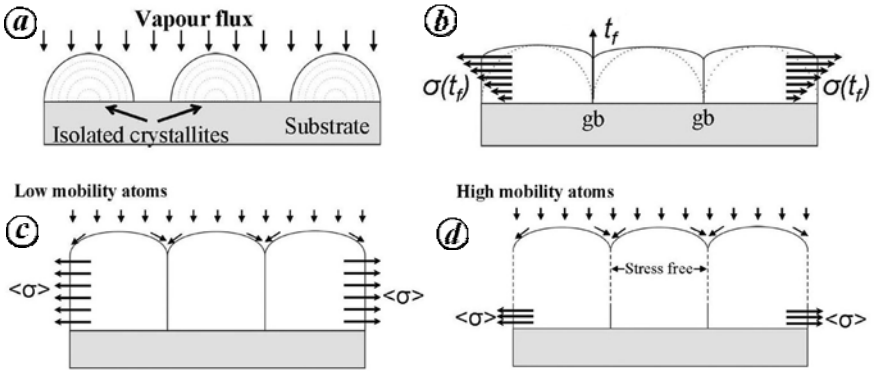

Figure 9. Schematic illustration of the growth stages associated with the Volmer–Weber growth mode. (***a***) Precoalescence stage. (***b***) Coalescence stage accompanied by the formation of grain boundaries (gb), showing the elastic displacement and stresses associated with forming a continuous film; and growth of polycrystalline film after the point of crystallite coalescence where the film grows in strained state in the case of low atom mobility (***c***), but in the case of high atom mobility (***d***), surface diffusion to the grain boundaries allows the stresses to be relaxed during subsequent growth.

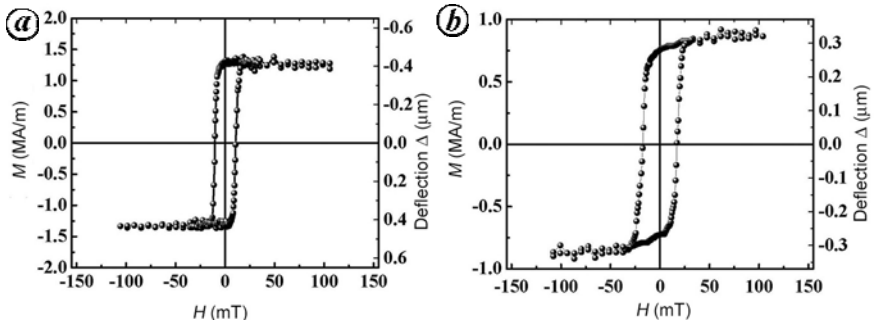

Figure 10. *M–H* curve of (120 ± 5) nm polycrystalline films of (***a***) Fe and (***b***) Co measured at 30°C (room temperature).

Magnetization measurement

After the stress measurement, Fe and Co samples were translated into the orthogonal magnetic field for magnetization measurement. Figure 10 *a* and *b* shows the *M–H* curves (measured at room temperature) of Fe and Co films of 120 nm thickness respectively. The hysteresis loops are obtained varying the magnetizing field (H_m) in a closed loop and measuring the substrate deflection in a deflecting magnetic field (B_{defl}) of 10 mT. The experimental values of the saturation magnetization of Fe and Co films are obtained as 1.21 ± 0.02 MA/m (coercivity: H_C = 10 mT) and 0.82 ± 0.02 MA/m (H_C = 17 mT) respectively. They are in good agreement with the values reported in the literature[23]. The saturation magnetization lies significantly below the bulk value (= 1.78 MA/m) probably due to considerable reduction in the Curie temperature.

Summary

Understanding of the correlation among various physical properties with morphology of thin films may be one of the major scientific and technological interests of the 21st century. The CBM can be used as a tool for this purpose. We have described the design and fabrication of a home-built CBM under HV conditions. We have discussed in detail the instrumentation. To establish the performance of our magnetometer for studying the film morphology as well as its magnetic property, we have demonstrated the measurement on some standard magnetic as well as non-magnetic materials. It is observed that a small variation in the deposition parameters (ambient pressure, residual gas composition, deposition rate, substrate temperature, substrate contamination, etc.) may result in a significant change in the film stress, which can be exploited to correlate the morphology with physical properties of the thin films. The versatility of the instrument lies in the fact that it can be used to measure the magnetization, magnetostriction and magnetocrystalline anisotropy of magnetic thin films along with the intrinsic stress during and after deposition. With our present set-up we could only measure the intrinsic stress and magnetization. But this may not be a limitation; it can be upgraded adding transverse and lateral translational degrees of freedom to the CBM device for the measurement of magnetostriction as well as magnetocrystalline anisotropy.

1. Klokholm, E. and Berry, B. S., *J. Electrochem. Soc.*, 1968, **118**, 823–826.
2. Hoffmann, R. W., *Physics of Thin Films* (eds Hass, G. and Thun, R. E.), Academic Press, NY, 1966, vol. 3.
3. Hoffmann, R. W., *Surf. Interface Anal.*, 1981, **3**, 62–66.
4. Doerner, M. F. and Nix, W. D., *CRC Crit. Rev. Solid State Mater. Sci*., 1988, **14**, 225–268.
5. Koch, R., *J. Phys. – Condense. Matter*, 1994, **6**, 9519–9550.
6. Campbell, D. S., *Handbook of Thin Film Technology* (eds Maissel, L. I. and Glang, R.), McGraw Hill, NY, 1970.
7. Murakami, M., Angelillo, J., Huang, H-C. W., Segmüller, A. and Kircher, C. J., *Thin Solid Films*, 1979, **60**, 1–90.
8. Ruud, J. A., Witvrouw, A. and Spaepen, F., *J. Appl. Phys*., 1993, **74**, 2517–2523.
9. Klockholm, E., *Rev. Sci. Instrum*., 1969, **40**, 1054–1058.
10. Hoffmann, R. W., *Thin Solid Films*, 1976, **34**, 185–190.
11. Koch, R., Leonhard, H., Thurner, G. and Abermann, R., *Rev. Sci. Instrum.*, 1990, **61**, 3859–3862.
12. Chaudhari, P., *J. Vac. Sci. Technol.*, 1972, **9**, 520–522.
13. Moske, M. and Samwer, K., *Rev. Sci. Instrum*., 1988, **59**, 2012–2017.
14. Laugier, M., *Thin Solid Films*, 1981, **75**, 213–219.
15. Abermann, R., *Vacuum*, 1990, **41**, 1279–1282.
16. Koch, R., Winau, D. and Rieder, K. H., *Phys. Scr*., 1993, **T49**, 539–543.
17. Falicov, L. M. *et al.*, *J. Mater. Res*., 1990, **5**, 1299–1340.
18. Bergholz, R., Ph D thesis, Technische Universität Clausthal, 1984.
19. Przybylski, M., Korecki, J. and Gradmann, U., *Appl. Phys. A*, 1991, **52**, 33–47.
20. Gerhardter, F., Li, Y. and Baberschke, K., *Phys. Rev. B*, 1993, **47**, 11204–11210.
21. Bader, S. D., *J. Magn. Magn. Mater*., 1991, **100**, 440–454.
22. Spagna, S., Sager, R. E. and Maple, M. B., *Rev. Sci. Instrum*., 1995, **66**, 5570–5576.
23. Weber, M., Koch, R. and Rieder, K. H., *Phys. Rev. Lett*., 1994, **73**, 1166–1169.
24. Sander, D., Enders, A. and Kirschner, J., *Rev. Sci. Instrum*., 1995, **66**, 4734–4735.
25. Koch, R., Dongzhi, H. and Das, A. K., *Phys. Rev. Lett.*, 2005, **94**, 146101(1)–(4).
26. Koch, R., *Surf. Coat. Technol.*, 2010, **204**, 1973–1982.
27. Koch, R., Das, A. K., Yamaguchi, H., Pampuch, C. and Ney, A., *J. Appl. Phys.*, 2004, **96**, 2773–2778.
28. Timoshenko, S. and Woinowsky-Krieger, S., *Theory of Plates and Shells*, McGraw Hill, Tokyo, 1959.
29. Du Trémolet de Lacheisserie, E. and Peuzin, J. C., *J. Magn. Magn. Mater*., 1994, **136**, 189–196.
30. Nix, W. D. and Clemens, B. M., *J. Mater. Res*., 1999, **14**, 3467–3473.
31. Finegan, J. D. and Hoffmann, R. W., *J. Appl. Phys*., 1959, **30**, 597–598.

ACKNOWLEDGEMENTS. We thank DRDO, India for providing financial support in the development of the CBM set-up. We also thank R. Koch, JKU, Austria for providing us the opportunity to visit his CBM laboratory and for sharing his experience and some critical components for the set-up and Dr Abhijit Majumdar, Institute for Physics, Germany for fabricating insulating rings for the CBM device. A.S. thanks CSIR, New Delhi for awarding Senior Research Fellowship.

Received 15 November 2011; accepted 28 January 2013

A. Sarkar, R. Adhikari and A. K. Das are in the Department of Physics and Meteorology, Indian Institute of Technology Kharagpur, Kharagpur 721 302, India; A. Sarkar and R. Adhikari are currently at Institut für Halbleiter- und Festkörperphysik Altenbergerstr. 69, A-4040 Linz, Austria.*

**e-mail: amal@phy.iitkgp.ernet.in*